The Duffing Oscillator

A Numerical Investigation of Duffing's
Non-Linear Dynamical System

Guy Leckenby

Project 1 for Theoretical Physics

Australian
National
University

College of Physical and Mathematical Sciences
The Australian National University
April 18, 2016

Contents

1 Introduction **1**

2 The Duffing Oscillator **2**

2.1 Dimensional Analysis 3

2.2 Limiting Cases 4

2.3 Frequency Profile and Hysteresis 5

2.4 Formulation as a Discrete Mapping 6

3 Fixed and Homoclinic Points **8**

3.1 Stability of Fixed Points 8

3.2 Stable and Unstable Manifolds 9

3.3 Homoclinic Points 10

4 Bifurcations and Cascades **12**

4.1 Periodic Orbits 12

4.2 Bifurcations 12

4.3 Cascades 14

4.4 Basin Boundaries 16

5 Chaos **18**

5.1 Lyapunov Exponents 18

5.2 Chaotic Attractors 19

5.3 Evolution of the Poincaré Section 21

6 Conclusion **23**

1 Introduction

This project is primarily designed to analyse chaotic systems and gather an appropriate understanding of the importance of chaotic motions to physics. As a result it is essential to understand the terminology used when discussing dynamical systems. According to Ott (2002, p. 6), one way to define a **dynamical system** is "a deterministic mathematical prescription for evolving the state of a system in time." This system will evolve in a *phase space* of N dimensions that characterises the system. The path through phase as the system is evolved is referred to as the *orbit* or *trajectory* of the system for a given set of initial conditions.

The most common dynamical systems studied at an undergraduate level are mostly in the linear regime and hence the analytic solutions produced, if bounded in finite phase space, will settle down to one of two generic behaviours; a steady state solution where the system ceases motion or a regular oscillation that is either periodic or quasiperiodic (Alligood et al. 1996, p. vi). However around 1975, scientists became interested in a further regime of dynamics, now called chaos, where erratic motion is observed that is not simply quasiperiodic or due to a large number of particles but is rather a rich behaviour in and of itself.

This new chaotic behaviour will be examined through the motions of the Duffing Oscillator which is particularly powerful due to its similarity with the standard linear damped driven oscillator. Thus there are many parallels and limiting cases which are familiar to the reader and allow for a more natural demonstration of the features of chaos. The Duffing Oscillator itself is not simply an equation that demonstrates chaos but is a powerful model that can be applied in many disciplines with diverse applications in neurology (Srebro, 1995) and economics (Kulkarni, 2012). With this in mind, it is essential to understand it's behaviours and characteristics and draw some useful predictions from the model.

2 The Duffing Oscillator

Fundamentally, the duffing oscillator is a nonlinear second-order ordinary differential equation given by (2.1) and produced from a symmetric quartic potential.

$$\ddot{x} + 2\gamma\dot{x} + \alpha x + \beta x^3 = F\cos(\omega t) \tag{2.1}$$

In terms of the parameters, the natural form has five;

- γ controls the size of the damping of the oscillator,
- α controls the stiffness which is resistance to elastic deformation,
- β controls the nonlinearity in the restoring force,
- F controls the amplitude of the driving,
- and ω controls the frequency of the driving.

The Duffing Oscillator has a nonlinear but symmetric restoring force give by $F_R = -\alpha x - \beta x^3$. Unlike the standard Simple Harmonic Oscillator, the nonlinearity in the Duffing Oscillator produces a quartic potential well,

$$U(x) = \frac{1}{2}\alpha x^2 + \frac{1}{4}\beta x^4, \tag{2.2}$$

pictured in Figure 2.1, that produces more complex motions. Note that it is required that $\alpha \leq 0$ and $\beta \geq 0$ otherwise the potential is either negative which is not a restorative force or lacks the double well form which generates the complex motions.

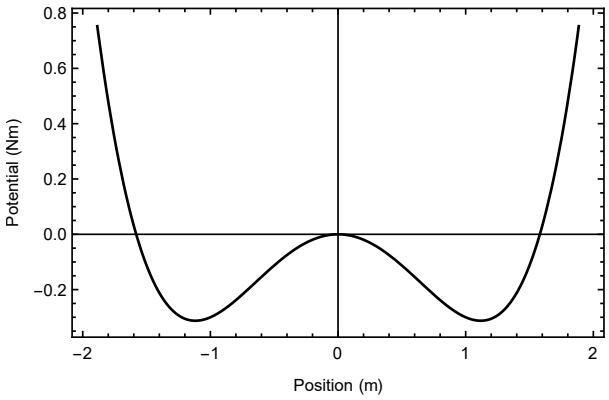

Figure 2.1: The potential of the Duffing Oscillator with $\alpha = -1$, $\beta = 0.8$.

Fundamentally, the Duffing Oscillator is the action of a point particle under a double well potential however it models many realistic systems well. Apart from the more complex neurological and economic applications mentioned above, a simpler driven torsional inverted pendulum is a good physical grounding studied in the Second Year Lab program at ANU (Corr, 2015) represented in Figure 2.2. The equation of motion of such a pendulum is

$$ml^2\ddot{\theta} = mg\sin\theta - kl\theta - \delta l\dot{\theta} + F_0\cos\omega t \tag{2.3}$$

where m is the mass of the weight, l is the length of the pendulum, δ is the damping coefficient, k is the spring coefficient, F_0 is the driving force amplitude and ω is the frequency of the driving. As the pendulum oscillates to angles that violate the small angle approximation, the next non-zero term in the McLaurin series must be included thus giving an approximation $\sin\theta \approx \theta - \frac{1}{6}\theta^3$. After algebraic manipulation, this produces the Duffing Equation (also implying, since $m, g, l, k > 0$, that $\alpha > 0$ and $\beta < 0$).

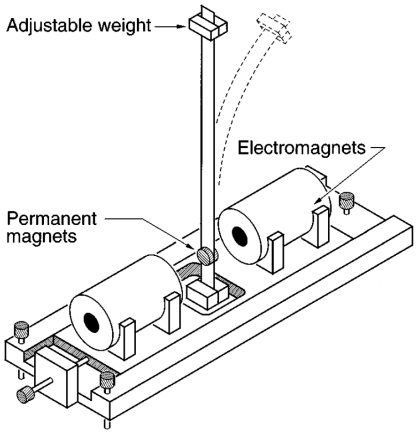

Figure 2.2: Inverted driven torsional pendulum (Berger & Nunes, 1997).

2.1 Dimensional Analysis

Whilst (2.1) is the most physically intuitive way of expressing the Duffing equation, it is not the simplest. In particular dimensional analysis can be used to simplify the number of parameters to five. This is done using the Buckingham-π theorem (MIT, 2013) which says that if an expression $f(q_1, \ldots, q_n) = 0$ contains n physically meaningful parameters with k fundamental dimensions, it can be simplified to an expression $\phi(\Pi_1, \ldots, \Pi_j) = 0$ in terms of $j = n - k$ dimensionless parameters called 'Pi groups'.

The Duffing Oscillator given in (2.1) has seven physical parameters,

$$x,\ \gamma,\ \alpha,\ \beta,\ F,\ \omega,\ \text{and}\, t.$$

Given that $\ddot{x}$ is a linear acceleration with units of $m\,s^{-2}$, it follows that each term in (2.1) must have these same units. Thus by deduction, it follows that these parameters respectively have the units

$$x : m,\ \gamma : s^{-1},\ \alpha : s^{-2},\ \beta : m^{-2}s^{-2},\ F : m\,s^{-2},\ \omega : s^{-1},\ \text{and}\ \ t : s.$$

Thus there are only two fundamental dimensions, m, s. Hence there exists a simplified expression for the Duffing equation with only five Pi groups.

Furthermore the Pi groups are known to be dimensionless by the Buckingham-π theorem. Any five Pi groups that include all the parameters will work. By inspection and using the methods suggested by MIT (n.d.), the following pi groups (with slightly more manageable names) were found;

$$\Pi_1 = y = \frac{x\sqrt{\beta}}{\omega}, \quad \Pi_2 = \tau = \omega t, \quad \Pi_3 = a = \frac{\gamma}{\omega}, \quad \Pi_4 = b = \frac{\alpha}{\omega^2}, \text{ and } \Pi_5 = G = \frac{F\sqrt{\beta}}{\omega^3}.$$

Note that each of the Pi groups is dimensionless and that every parameter has been included. Substituting in y and τ first and noting that

$$\frac{\mathrm{d}x}{\mathrm{d}t} = \frac{\mathrm{d}x}{\mathrm{d}\tau}\frac{\mathrm{d}\tau}{\mathrm{d}t} = \frac{\omega^2}{\sqrt{\beta}}\frac{\mathrm{d}y}{\mathrm{d}\tau} \qquad \frac{\mathrm{d}^2x}{\mathrm{d}t^2} = \frac{\mathrm{d}}{\mathrm{d}\tau}\left(\frac{\omega^2}{\sqrt{\beta}}\frac{\mathrm{d}y}{\mathrm{d}\tau}\right)\frac{\mathrm{d}\tau}{\mathrm{d}t} = \frac{\omega^3}{\sqrt{\beta}}\frac{\mathrm{d}^2y}{\mathrm{d}\tau^2},$$

equation (2.1) transforms to

$$\frac{\omega^3}{\sqrt{\beta}}\ddot{y} + \frac{2\gamma\omega^2}{\sqrt{\beta}}\dot{y} + \frac{\alpha\omega}{\sqrt{\beta}}y + \frac{\omega^3}{\sqrt{\beta}}y^3 = F\cos\tau$$

$$\ddot{y} + \frac{2\gamma}{\omega}\dot{y} + \frac{\alpha}{\omega^2}y + y^3 = \frac{F\sqrt{\beta}}{\omega^3}\cos\tau$$

$$\ddot{y} + 2a\dot{y} + by + y^3 = G\cos\tau$$

where the terms $\dot{y}$ and $\ddot{y}$ are with respect to τ. Thus it follows that this is the desired expression $\phi(\Pi_1, \ldots, \Pi_5) = 0$ and that ϕ is equivalent to the Duffing Oscillator (2.1) by the Buckingham-π theorem.

Note that using the Buckingham-π theorem via inspection requires some foresight in terms of the most convenient expression. In this case, the choices were motivated by Zhao's (2014) choices for simplification. Furthermore note that from this point forward, when the Duffing Oscillator is referred to, the form of equation (2.4),

$$\ddot{x} + a\dot{x} + bx + x^3 = F\cos t, \tag{2.4}$$

will be used knowing that it is equivalent to (2.1) (the factor of 2 has been absorbed into a for conciseness). Further note that because of the requirement that $\alpha \leq 0$ it is required that $b \leq 0$.

2.2 Limiting Cases

It is insightful to investigate the limiting cases of any system to ensure it collapses to a logical point. In this case, it is interesting to investigate the behaviour of the parameters under the limits $a, b, F \to 0$ (the infinite limit is less interesting). Revising what each parameter controls physically under the simplification, a now controls the strength of the damping, b determines to nonlinearity of the restorative force and F determines the amplitude of the driving. Note that not all limit combinations will be considered, only those that demonstrate simple behaviour.

Suppose $a, F \to 0$. Then there is no damping and the Duffing Oscillator becomes a **simple nonlinear oscillator**. Thus a nonlinear trajectory is expected due to the quartic potential well seen in Figure 2.1. As visible in Figure 2.3(a), the phase space diagram for this setup, the pendulum increases velocity and position as it falls into the potential well, inverts velocity as it reaches the peak of the swing, then accelerates again over the centre of the potential. The nonlinearity of the quadratic potential produces the 'pinched in' velocity of the trajectory as the particle travels over the peak in the centre of the potential. This can be attributed to the nonlinearity as by setting $b \to 0$ in Figure 2.3(a), no 'pinching' occurs.

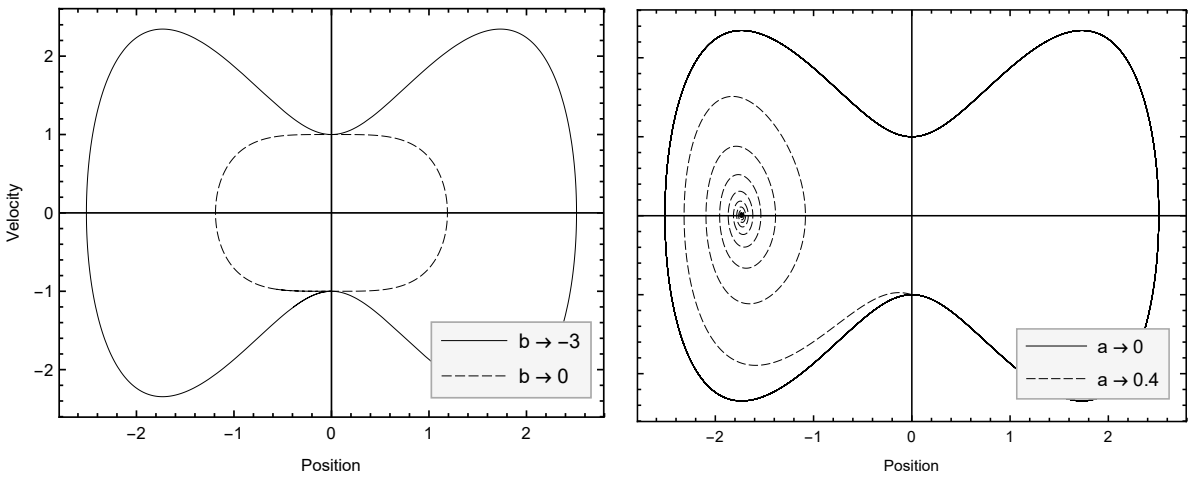

(a) Simple nonlinear oscillator. **(b)** Damped nonlinear oscillator.

Figure 2.3: Phase space profiles for various limits of the Duffing Oscillator.

If a is reintroduced such that only $F \to 0$, then the Duffing Oscillator collapses to a **damped nonlinear oscillator**. With the damping term introduced, the particle loses energy until it no longer can oscillate between potential wells. The long term behaviour involves decaying to a stable fixed point in whatever well it has been trapped. This is seen in Figure 2.3(b) where for positive a, the solution decays to the fixed point.

The fixed points of the nonlinear potential have an important impact on the limiting cases. In particular setting the potential $U(x) = \frac{1}{2}bx^2 + \frac{1}{4}x^4 = 0$, three fixed points are found, $x = 0, \pm\sqrt{b}$. $x = 0$ is unstable whilst $x = \pm\sqrt{b}$ are stable. Thus in the damped case, it is expected that the long term behaviour of the system will be to settle at either $x = \pm\sqrt{b}$. If the system is undamped also, the trajectory in phase space, which has constant energy, will encompass one or both of the stable fixed point, depending on the initial energy.

2.3 Frequency Profile and Hysteresis

As the Duffing Oscillator is a driven oscillator, it naturally has a frequency response curve however due to the nonlinear nature of the oscillator, it behaves quite differently from the traditional frequency response. The following results are discussed here because they are generated primarily from the nonlinearity of the Duffing Oscillator rather than the chaotic motions directly.

The frequency response of a driven oscillator is the response of the amplitude of oscillation with respect to the driving frequency. In particular the system is expected to exhibit a *resonance frequency* ω_0 where the amplitude is maximised with the response falling off as the frequency gets further away. The Duffing Oscillator behaves slightly differently. To analyse the frequency response of the oscillator, it is studied under the assumption that the steady state response of the system is sinusoidal and given by

$$x(t) = \mathcal{A}(\omega)\cos(\omega t - \theta). \tag{2.5}$$

To obtain the frequency response, (2.5) is substituted into (2.1) and then the coefficients of the orthogonal functions sine and cosine are equated upon which the expressions are squared and added to produce (2.6) (Das, 2002),

$$\mathcal{A}^2\Big[(1-\omega^2) + \frac{3}{4}\mathcal{A}^2\Big]^2 + (2\gamma\mathcal{A}\omega)^2 = F^2. \tag{2.6}$$

(2.6) is biquadratic in ω and can be solved analytically for $\mathcal{A}$ as a function of ω if negative solutions are discarded as nonphysical. This produces three individual solutions, given numerical γ and F values are provided, which can be seen in Figure 2.4. The three solutions connect

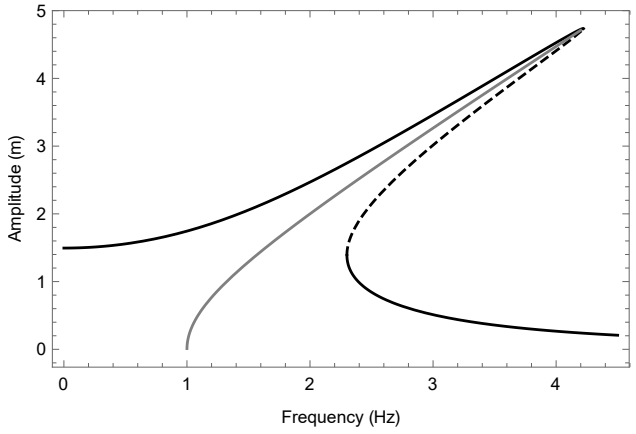

Figure 2.4: Frequency response curve for the Duffing Oscillator with $\gamma = 0.1,\ F = 4$.

continuously to produce the black curve, the middle solution is dashed to separate the three, however they are all independent solutions. The grey solution represents the free oscillations and its departure from vertical measures the *anisochronism* or nonlinearity of the oscillator (Sconza & Torzo, 2002). As evident, the response peak bends to the right, deviating from the vertical peak expected in linear oscillations.

This deviation produces the interesting result that (in the example case) with $2.3 < \omega < 4.2$ the amplitude has three possible roots. What happens physically is that if the frequency is low and increased, the amplitude follows the upper solution curve until the maximum value (4.2 in Figure 2.4) is reached and then it drops and continues on the lower curve. If the frequency is high and reduced, then the amplitude follows the lower curve until the turning point is reached (2.3 in Figure 2.4) where it jumps to the upper curve and continues. The dashed middle curve thus cannot be observed experimentally but remains a solution. This phenomena is known as *amplitude jumps in forced nonlinear oscillations* (Sconza & Torzo, 2002).

Amplitude jumping is an example of a hysteretic behaviour. **Hysteresis** is broadly the dependence of a system on its history, that is to determine its current state, its history must be known (Sethna, 1994). Is this situation, whether the frequency was increased or decreased to get to the current driving frequency must be known to determine which amplitude the oscillator exhibits.

Thus the hysteretic behaviour of the Duffing Oscillator yet again demonstrates its nonlinearity and how it can demonstrate exotic behaviours.

2.4 Formulation as a Discrete Mapping

A dynamical system that evolves with time can either have a continuous or discrete formulation. A continuous time system is referred to a *flow* and is typically represented by a differential equation whilst discrete time involves a *mapping* that evolves the system as a countable sequence. So far the Duffing Oscillator has been introduced in continuous time however many chaotic phenomena are much simpler to introduce and explore in terms of a discrete mapping. Hence it is useful to construct a discrete time mapping from our differential equation.

There are two different formulations of converting a flow to a discrete system, the **Poincaré surface of a section** method or the **time-T sampling** method (Ott, 2002). The time-T method is the simplest and simply involves sampling the flow at discrete times $t_n = t_0 + nT$ for some T chosen for convenience. Thus a flow $x(t)$ yields a discrete orbit $x_n \equiv x(t_n)$. The quantity x_{n+1} is uniquely determined by x_n as x_n is simply used as initial conditions and then integrated to a time T. Thus the time-T map is invertible as it is one-to-one and onto throughout the phase space.

The Poincaré map is slightly more complicated but much more elegant. Poincaré realised that many behaviours of a system could be determined by considering a subspace of the phase space, most commonly a plane, by tracking the intersections of the orbit with this subspace. Consider the plane S in Figure 2.5 which is termed the *surface of a section*. Let A represent the k^{th} rightward piercing of the plane and C be the $k + 1^{th}$ right piercing. Then the Poincaré map is the map $P(A) = C$. That is $x_{k+1} = C$ is uniquely determined by $x_k = A$ by following the solution from A until it again pierces the plane from the right at C (Alligood et al., 1996).

The difference between the Poincaré map and the time-T map is that the time-T map is *stroboscopic* (meaning that the values are collected at equal time intervals) whilst the Poincaré map depends on when the solution pierces the surface of a section. Furthermore the Poincaré map reduces the dimension of a dynamical system from k in continuous form to $k-1$ in discrete form whilst the time-T map retains the dimensionality k.

Turning to the model of the Duffing Oscillator presented in (2.4), the formulation presents a

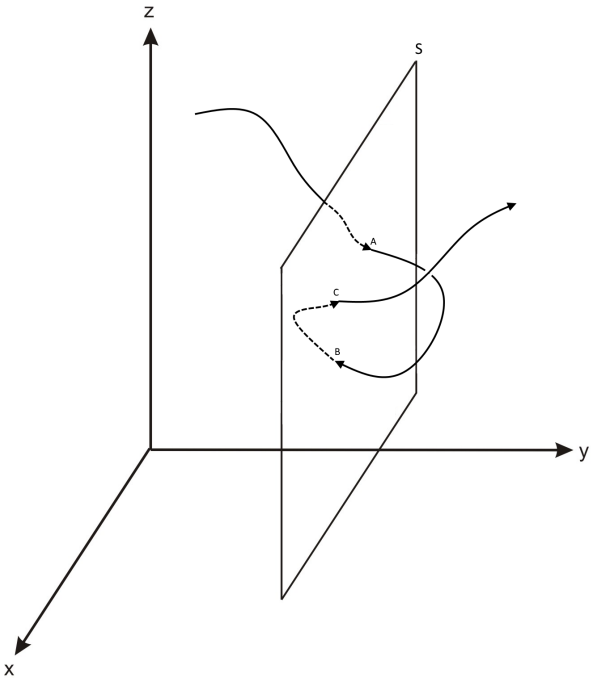

Figure 2.5: A Poincaré map derived from a continuous time solution.

continuous time solution by solving the second order nonlinear ordinary differential equation. This can be transformed into a system of first order linear autonomous ODE's presented in (2.7) using the substitutions $x_1 = \dot{x}$, $x_2 = x$ and $x_3 = t$.

$$\begin{aligned} \dot{x}_1 &= F\cos x_3 - bx_2 - x_2^3 - ax_1 \\ \dot{x}_2 &= x_1 \\ \dot{x}_3 &= 1. \end{aligned} \tag{2.7}$$

Then since $x_3 = t$ can be treated as an angle in phase space, x_3 is equivalent to $\overline{x}_3 = x_3 \mod 2\pi$. Choosing the surface of a section to be $\overline{x}_3 = 0$, the surface of a section is crossed at time $t = 0, 2\pi, 4\pi, \ldots$ which is particularly interesting as it is also stroboscopic. Thus the Poincaré map chosen for the Duffing Oscillator is equivalent to the time-2π map.

This equivalence of the Poincaré map and the time-2π map for the Duffing Oscillator has deeper implications that will be explored in the next section. However for the current purpose, it suffices to say that when the discrete mapping of the Duffing Oscillator is mentioned, the time-2π map is being referred to; constructed by numerically solving the ODE's for 2π time steps.

3 Fixed and Homoclinic Points

The Duffing Oscillator exhibits a wide variety of behaviours that can be nonchaotic, transitory, and chaotic. It is a property of nonchaotic systems that as time evolves, they will approach a steady state, whether this be a stable point or a stable oscillation. Hence it is interesting to investigate whether the Duffing Oscillator exhibits the same behaviours.

First however, the concept of a *fixed state* needs to be defined. A fixed state is one where the system does not change with evolution in time. These fixed states can either manifest as a zero (point) or one (curve) dimensional manifold in the two dimensional projection phase space. Projection phase space will be used regularly because it is easier to visualise. However note that whilst solutions may cross in projection phase space, they don't cross in true phase space because of the third dimension of time. A point implies the particle is at rest whilst a curve implies a periodic oscillation.

3.1 Stability of Fixed Points

Stability of fixed states is significant because small perturbations in reality mean that the behaviour near a fixed state needs to be examined. In particular, solutions will either fall away from or towards a fixed state depending the stability of the neighbourhood. An ε-neighbourhood is defined below.

Definition 3.1 *Let* $\mathbf{x}$ *and* $\mathbf{p}$ *exist in phase space* $\mathbb{R}^n$*. Then the* ε*-neighbourhood is the set*

$$N_\varepsilon(\mathbf{p}) = \{\mathbf{x} \in \mathbb{R}^n : |\mathbf{x} - \mathbf{p}| < \varepsilon\}.$$

For this section, it is more intuitive to consider the solutions in the time-2π map because fixed states including periodic oscillations will be represented by a single point and neighbourhoods can be visualised by circles rather than complex torus's.

With this in mind, fixed states can be classified depending on how the ε-neighbourhood behaves under mapping. If an ε-neighbourhood of a fixed point collapses under mapping, then the fixed point is called a **source**. If the ε-neighbourhood expands, then it is a **sink**. Finally if the ε-neighbourhood does a combination of both, it is a **saddle** (Alligood et al., 1996, p. 9). Sinks are called stable because points near them will be stabilised by the sink. For sources and saddles however, points are mapped away from the fixed point and thus are called unstable. These definitions are exhibited in Figure 3.1.

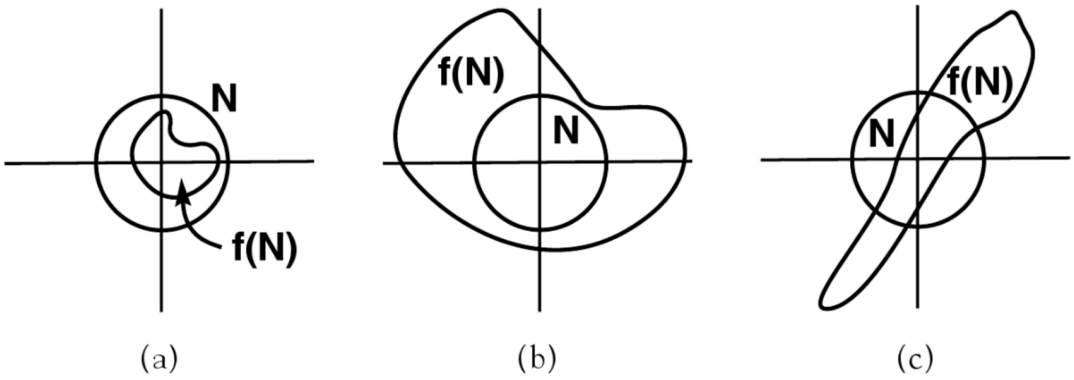

Figure 3.1: Local dynamics near a fixed point (Alligood et al., 1996, p. 59).

To find a numerical method for determining the stability of fixed points requires the Jacobian matrix which is an analogue of the derivative in multidimensional space.

Definition 3.2 *If* $\mathbf{f}$ *is a map on* $\mathbb{R}^n$ *and* $\mathbf{p} \in \mathbb{R}^n$*, then the* ***Jacobian matrix*** *of* $\mathbf{f}$ *at* $\mathbf{p}$*, denoted by* $\mathbf{Df}(\mathbf{p})$ *is*

$$\mathbf{Df}(\mathbf{p}) = \begin{pmatrix} \frac{\partial f_1}{\partial x_1} & \cdots & \frac{\partial f_1}{\partial x_n} \\ \vdots & \ddots & \vdots \\ \frac{\partial f_n}{\partial x_1} & \cdots & \frac{\partial f_n}{\partial x_n} \end{pmatrix}.$$

Given this, *linear stability analysis* provides a method for determining the stability of fixed points (Weisstein, n.d.).

Theorem 3.1 *Let* $\mathbf{f}$ *be a map on* $\mathbb{R}^n$ *and let* $\mathbf{p}$ *be a fixed point of* $\mathbf{f}$*. Then*

1. *If the real component of each eigenvalue of* $\mathbf{Df}(\mathbf{p})$ *is negative, then* $\mathbf{p}$ *is a sink.*
2. *If the real component of each eigenvalue of* $\mathbf{Df}(\mathbf{p})$ *is positive, then* $\mathbf{p}$ *is a source.*
3. *If the real component of at least one eigenvalue of* $\mathbf{Df}(\mathbf{p})$ *is negative and another positive, then* $\mathbf{p}$ *is a saddle.*

As seen in (2.7), the duffing oscillator forms a three dimensional autonomous system. This system has the following Jacobian matrix (Kanamaru, 2008).

$$\mathbf{Df}(\mathbf{x}) = \begin{pmatrix} 0 & 1 & 0 \\ -b - 3x^2 & -a & F\sin t \\ 0 & 0 & 1 \end{pmatrix} \tag{3.1}$$

From the potential well, the fixed points are known to be $\mathbf{x} = (0,0)$, $(\pm\sqrt{b}, 0)$ in phase space (time is excluded). The eigenvalues of (3.1) are

$$(0,0): \ \lambda = 1, \frac{1}{2}\left(-a \pm \sqrt{a^2 - 4b}\right), \qquad (\pm\sqrt{b}, 0): \ \lambda = 1, \frac{1}{2}\left(-a \pm \sqrt{a^2 - 4b - 12b^2}\right).$$

Each fixed point has an eigenvalue 1 associated with the redundancy of the time substitution. It is evident that the stability of the fixed points depends on the parameters chosen. However for most parameters that are considered in this report, indeed the ones that produce the interesting behaviour, $(0,0)$ corresponds to an unstable saddle and $(\pm\sqrt{b}, 0)$ are both sinks. This is seen if the parameters $(a \to 0.5, b \to -1)$ into the eigenvalues. Then for $(0,0): \lambda = 1, -1.28, 0.78$ which is classified as a saddle and $(\pm\sqrt{b}, 0): \lambda = 1, -0.25 - 1.39i, -0.25 + 1.39i$ which are classified as sinks.

A reminder that when 'fixed points' are mentioned, they are points only under the time-2π map and actually represent fixed solution curves which pass through the same point every 2π (the fact that not all fixed solutions have period 2π is addressed in Section 4.1).

3.2 Stable and Unstable Manifolds

Sinks and sources are fairly straightforward in terms of the behaviour near them; they attract and repel respectively. In terms of sets, sources repel all points however sinks may attract only a subset. This subset of phase space that is eventually attracted to the sink is called its *basin of attraction* and represents the set of points that will have settled at the sink in the infinite time limit.

Saddles are different and more interesting because they attract some points but repel others. This is formalised in the concept of a stable and unstable manifold (Alligood et al., 1996, p. 78).

Definition 3.3 *Let* $\mathbf{f}$ *be a diffeomorphism (smooth, invertible) and* $\mathbf{p}$ *be a saddle point. Then the* ***stable manifold*** *denoted* $\mathcal{S}(\mathbf{p})$ *and the* ***unstable manifold*** *denoted by* $\mathcal{U}(\mathbf{p})$ *are given by*

$$\mathcal{S}(\mathbf{p}) = \{\mathbf{x} : \lim_{n\to\infty} |\mathbf{f}^n(\mathbf{x}) - \mathbf{f}^n(\mathbf{p})| = 0\} \qquad \mathcal{U}(\mathbf{p}) = \{\mathbf{x} : \lim_{n\to\infty} |\mathbf{f}^{-n}(\mathbf{x}) - \mathbf{f}^{-n}(\mathbf{p})| = 0\}.$$

Note that all points near a saddle except the stable manifold will diverge however not every other point constitutes the unstable manifold. Most points are simply deflected.

The stable and unstable manifolds are important because they inform the **stable manifold theorem** which will be used to draw conclusions about chaos. In particular, one formulation is presented by Alligood et al. (1996, p. 403) below.

Theorem 3.2 *(Stable Manifold Theorem.) Let* $\mathbf{f}$ *be a diffeomorphism of* $\mathbb{R}^2$ *and assume that* $\mathbf{f}$ *has a saddle* $\mathbf{p}$ *such that* $\mathbf{Df}(\mathbf{p})$ *has one eigenvalue with* $\mathrm{Re}(\lambda_1) < 0$ *and the other* $\mathrm{Re}(\lambda_2) > 0$ *with eigenvectors* $\mathbf{v}_1$ *and* $\mathbf{v}_2$ *respectively. Then both the stable manifold* $\mathcal{S}$ *and the unstable manifold* $\mathcal{U}$ *of* $\mathbf{p}$ *are one-dimensional manifolds (curves) that contain* $\mathbf{p}$*. Furthermore* $\mathbf{v}_1$ *is tangent to* $\mathcal{S}$ *and* $\mathbf{v}_2$ *is tangent to* $\mathcal{U}$*.*

3.3 Homoclinic Points

Generally, the stable and unstable manifolds of a saddle point will not intersect and many early dynamicists assumed that they could never cross. It is true that the (un)stable manifold cannot cross itself or any other (un)stable manifold but there are no restrictions on the stable and unstable manifolds intersecting (Alligood et al, 1996, p. 85), in fact, these define **homoclinic points**.

Definition 3.4 *If* $\mathbf{f}$ *is an invertible map on* $\mathbb{R}^n$ *and* $\mathbf{p}$ *is a saddle point, then a point* $\mathbf{x}$ *in both the stable and unstable manifold of* $\mathbf{p}$ *is called a* ***homoclinic point****.*

The implications of homoclinic points are extremely complex and only a brief glimpse will be presented here. If further investigation is required, then Lenci and Rega (2011, p. 219-76) present an exhaustive investigation into the effects of homoclinic points of the Duffing Oscillator. What can be said is that if there exists a single homoclinic point, then there must be infinitely many and there existence implies chaotic orbits (Alligood et al., 1996, p. 413). This is a result of the Smale-Birkhoff theorem which implies that fractal basin boundaries, sensitivity to initial conditions, chaotic transience, and the presence of chaotic saddles (Lenci & Rega, 2011, p. 256) all occur due to the existence of a homoclinic intersection.

Calculation of the stable and unstable manifolds cannot be done analytically for the Duffing Oscillator so computational approximations are used instead. Unfortunately, these algorithms

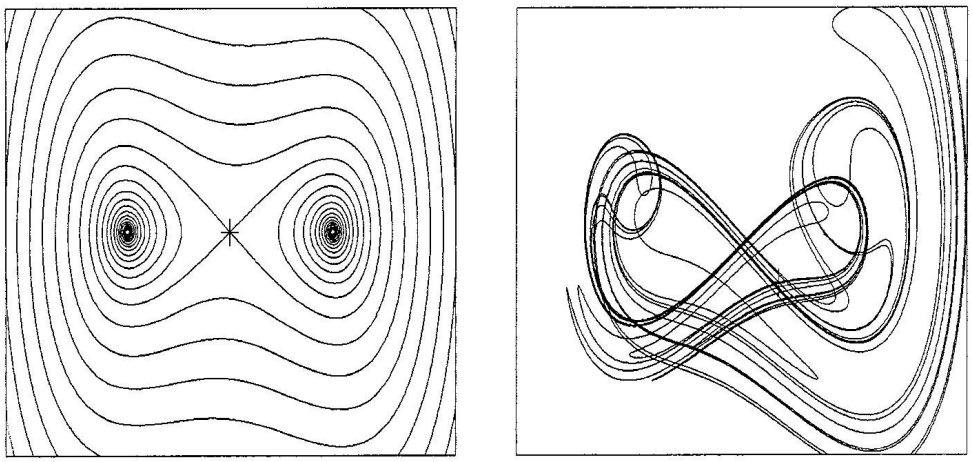

Figure 3.2: Stable and unstable manifolds for the time-2π map (Alligood et al., 1996, p. 59).

are quite in depth and beyond the scope of this project however Mancho et al. (2003) investigate such methodology. Instead, Alligood et al. (1996, p. 413) provides a calculation of these manifolds for $a \to 0.1, b \to -1$ and $F \to 0.3$ in Figure 3.2(b). As evident there are many homoclinic points and the stable manifold somewhat resembles the associated chaotic attractor. Note that in the unforced case, the stable manifold forms the basin boundary whilst the unstable manifold decays into the sinks as seen in Figure 3.2(a).

4 Bifurcations and Cascades

The fixed points investigated in Section 3.1 were the fixed points of the potential, that is the unforced Duffing Oscillator. When the forcing parameter is increased, the fixed points evolve from steady state points into oscillatory motion in continuous phase space. These motions are called **limit cycles** for when the forcing is low enough and the system is not exhibiting chaos, all orbits approach the limit cycle under infinite time.

These limit cycles have a period of 2π as the motion has synchronised with the period of the forcing. Hence under the time-2π map, each limit cycle can be characterised by a single point as the limit cycle returns to the same coordinates every 2π. These limit cycles are the new sinks because each orbit tends to them including the origin. Whilst the basins of attraction begin to be incurred upon with increasing F, under small forcing they still largely resemble Figure 3.2(a) and thus which basin the orbit originated from determines which of the two limit cycles the system will stabilise at, the positive or negative well.

4.1 Periodic Orbits

Whilst the limit cycles synchronise with the forcing period, there's nothing to prevent limit cycles existing with higher periods of integer multiples of 2π. These would be orbits that return to the same point in the Poincaré section every k iterations for example. Formally, a **periodic point of period** k is a fixed point under k iterations of the map f such that $f^k(p) = p$. For the Duffing Oscillator under the time-2π map, this means that the orbit returns to the same point in projected phase space every $2k\pi$ intervals of time.

These periodic orbits are seen in the Duffing Oscillator as the forcing amplitude is varied. For low forcing amplitude, a single limit cycle exists and the orbit has period 1. For higher forcing amplitudes, two or four or even more limit cycles appear in the projected phase space indicating higher period orbits. These limit cycles are seen in Figure 4.1 which shows a period 1, 2 and 4 orbit. As evident in Figure 4.1(d), the Poincaré section shows the various orbits piercing in k different places before repeating.

4.2 Bifurcations

In the above analysis of periodic orbits of the Duffing Oscillator, the forcing amplitude F was changed to produce higher periodic orbits. When F is increased, periodic orbits become unstable and higher periodic orbits replace them in a process called **bifurcation**. Consider the following definition (Alligood et al., 1996, p. 448).

Definition 4.1 *A **one-parameter family** of maps on $\mathbb{R}^n$ is a set of maps $\mathbf{f}_a(\mathbf{x})$, one for each value of a belonging to an interval I of real numbers. Then $\mathbb{R}^n$ is called the* state space *and I is the* parameter space*.*

There are two generic types of bifurcations (others include transcritical, pitchfork and Hopf bifurcations) called *saddle-node bifurcations* and *period doubling bifurcations*. Saddle-node bifurcations describe the transition where a system with no stable states gains two stable states, an unstable saddle and a sink, by varying a. Since the Duffing Oscillator already has at least two stable states (starting at $(x, v) = (\pm\sqrt{b}, 0)$) for small values of F, saddle-node bifurcation does not occur. Hence period doubling bifurcation is much more interesting.

Period doubling bifurcation occurs when a presently stable orbit transitions to unstable, for example a sink turns into a saddle. As a result two new stable orbits are born and the period of the orbit doubles. A period doubling bifurcation on a period k orbit results in a period $2k$

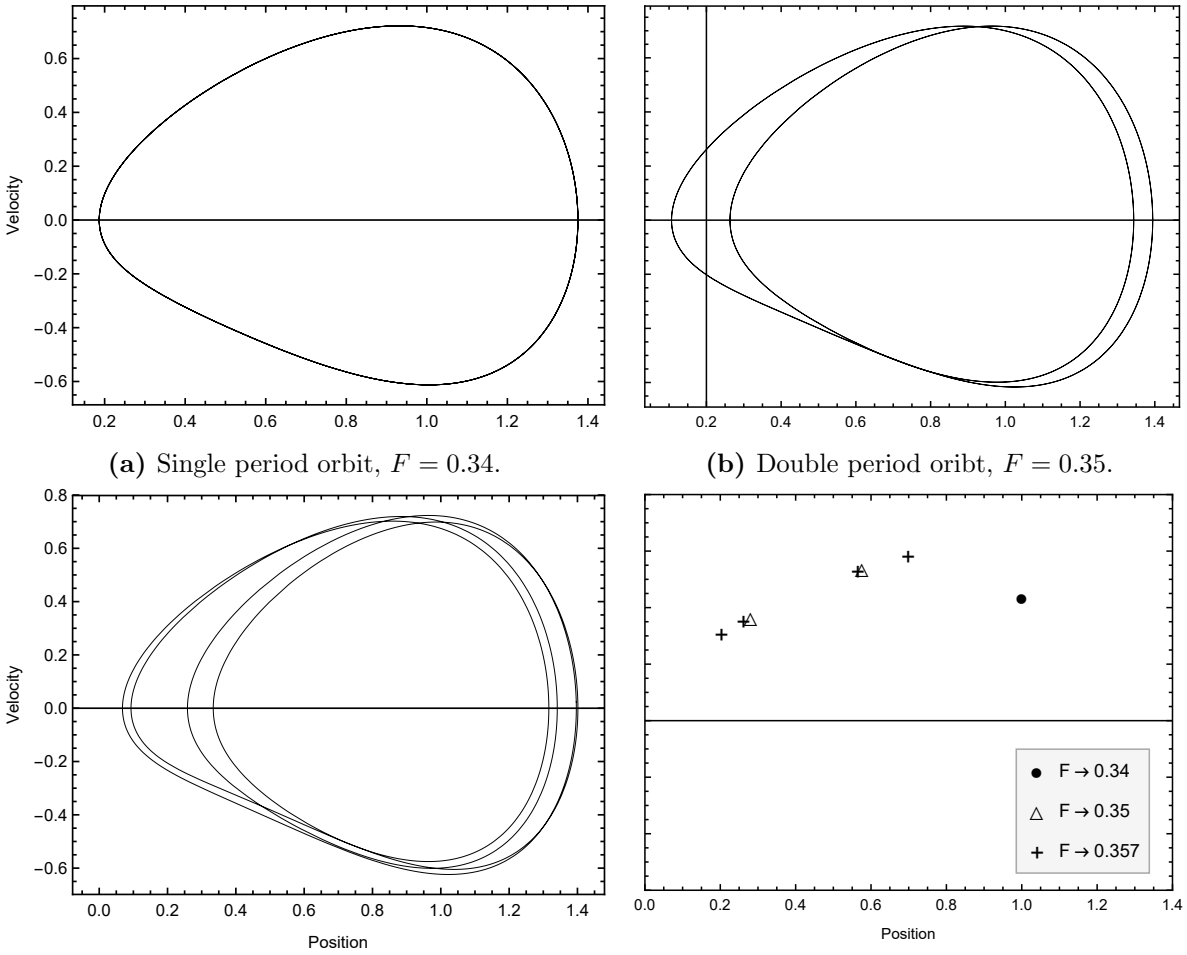

(a) Single period orbit, $F = 0.34$.

(b) Double period oribt, $F = 0.35$.

(c) Quadruple period orbit, $F = 0.357$.

(d) Poincaré points of each orbit.

Figure 4.1: Multiple period orbits of the Duffing oscillator. Subfigures (a) - (c) show the limit cycles, (d) shows their Poincaré section demonstrating the multiple periods.

orbit such that all period doubling occurs at the same parameter value. The exact reason for the period doubling involves an eigenvalue of the Jacobian crossing -1 at a nonzero rate. In Figure 4.2, a saddle-node bifurcation occurs at A whilst a period doubling bifurcation occurs at B. Note that the fixed point still continues after the period doubling, just that it changes from stable to unstable.

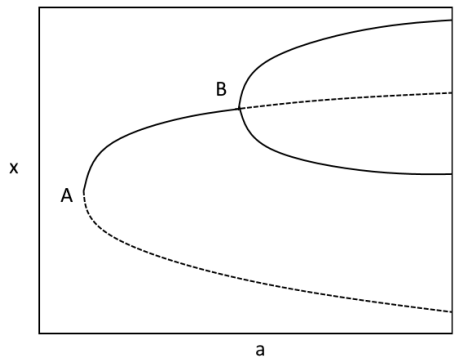

Figure 4.2: Saddle-node and period doubling bifurcations. Stable orbits are solid, unstable are dashed.

4.3 Cascades

Cascades of period doubling bifurcations have been seen in the great majority of low-dimensional systems that exhibit chaotic behaviour (Alligood et al., 1996, p. 499) and the Duffing Oscillator is no exception. This is where a stable orbit undergoes an infinite series of period doubling and is otherwise known as the period doubling route to chaos. The cascade for Duffing Oscillator with the forcing amplitude as the parameter is given in Figure 4.3. As evident, you can see clearly the first three bifurcations before they are lost in the resolution. However Figure 4.3(b) shows

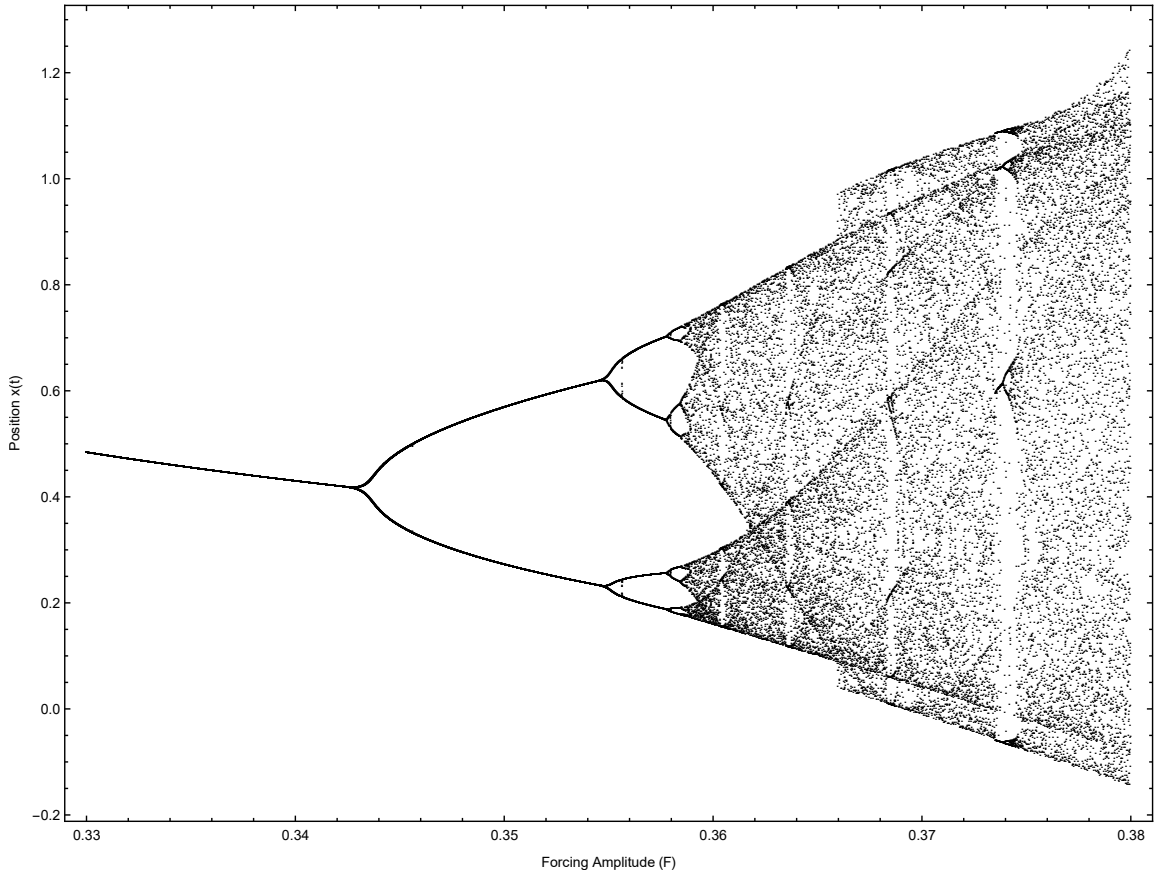

(a) The full cascade.

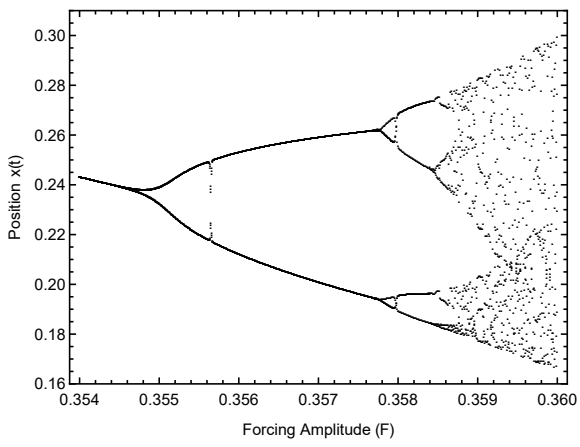

(b) A magnification of the lower second bifurcation.

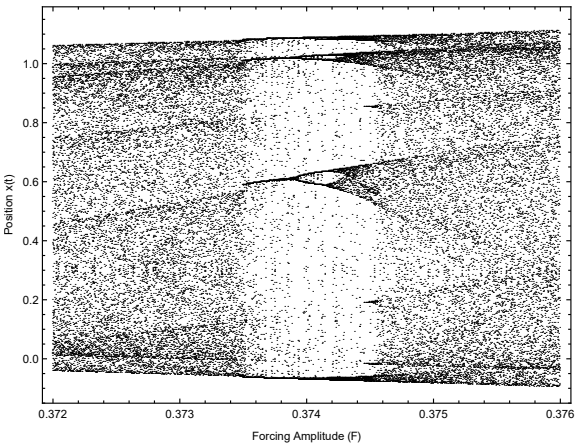

(c) A period window appearing later in the cascade.

Figure 4.3: Cascade of the Duffing Oscillator via the projected Poincaré section of position for $a \to 0.5, b \to -1$.

a magnification of the lower second bifurcation and the image looks markedly similar to Figure 4.3(a) such that we could say the cascade appears fractal which will be discussed in Section 5.4.

The cascade eventually approaches an infinite period in finite F and at this point, the attractors are no longer periodic with period k but rather dense (uncountably infinite) and are thus chaotic attractors. Due to the complex nature of the cascade, with very small changes in the family parameter, the attractor can discontinuously change in size. This is what is seen in periodic windows like in Figure 4.3(c) where an apparently infinite chaotic attractor collapses back to a period k orbit. This can be seen as the bifurcations of the f_F^k one-parameter family map and thus they then proceed to bifurcate again to infinity.

As the periodicity increases with the cascade,the limit cycles look more chaotic. In Figure 4.4 a variety of limit cycles can be seen throughout the cascade. In Figure 4.4(a), the limit cycle is still bound to the right well and is simply a very high k period orbit. In Figure 4.4(b), the limit cycle is of a periodic window and hence has collapsed back into a low period k orbit. Figures 4.4(c) & (d) are simply the projected phase space diagrams of chaotic orbits. The orbit has escaped one well and now oscillates between both. These orbits have infinite period and appear to be chaotic motion.

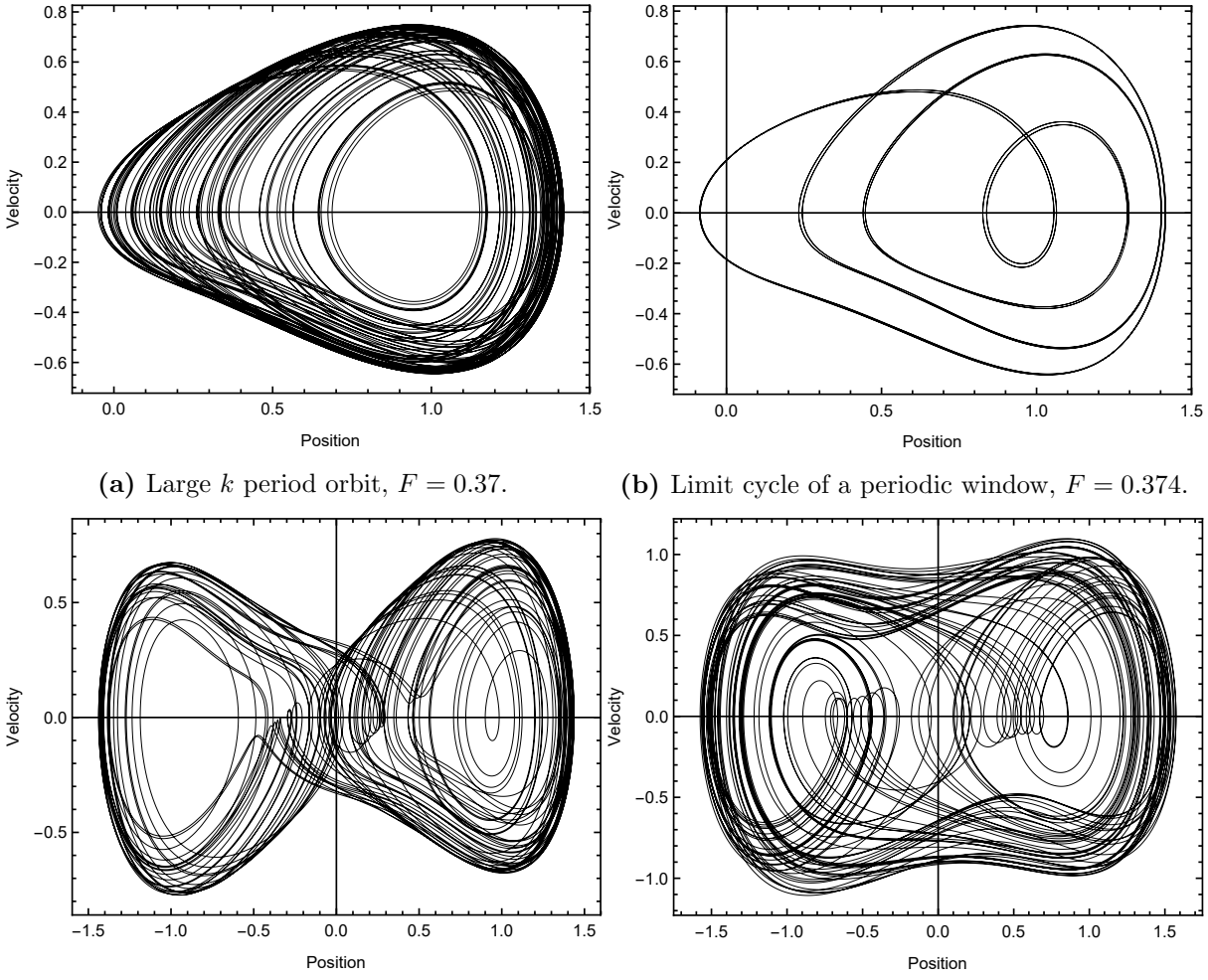

(a) Large k period orbit, $F = 0.37$.

(b) Limit cycle of a periodic window, $F = 0.374$.

(c) Complex limit cycle, $F = 0.4$.

(d) Chaotic orbit, $F = 0.7$.

Figure 4.4: The chaotic orbits during the cascade.

The fact that the size of the bifurcations in Figure 4.3(a) diminish so quickly suggests that there is probably some sort of scaling occurring. In 1978, M. Feigenbaum noted that the ratios of the distances between two successive bifurcations was constant (Alligood et al., 1996, p. 500). He derived this number to be, where a_n is the parameter value of the n^{th} bifurcation,

$$\lim_{n\to\infty} \frac{a_{n-1} - a_{n-2}}{a_{n-1} - a_n} = 4.669201609\ldots$$

which is today called Feigenbaum's constant. In Table 1 are the progressive values of the bifurcations and an estimate of Feigenbaum's constant.

Table 1: Feigenbaum's constant estimation.

n	a	FC
1	0.3429	
2	0.35463	
3	0.357775	3.72973
4	0.358460	4.59124

Finally, it is important to note that the bifurcation diagram in Figure 4.3(a) is a projection of the position coordinate of phase space only, such that the velocity was set to zero. This is because the important dynamics can be discerned quite clearly which is not possible for a 3D plot. However Figure 4.5 shows a 3D plot of the bifurcation regardless. What is particularly insightful about this diagram is that it shows how in full phase space the bifurcations cascade into the chaotic attractor represented in Figure 5.1(b) demonstrating that this really is the period doubling route to chaos.

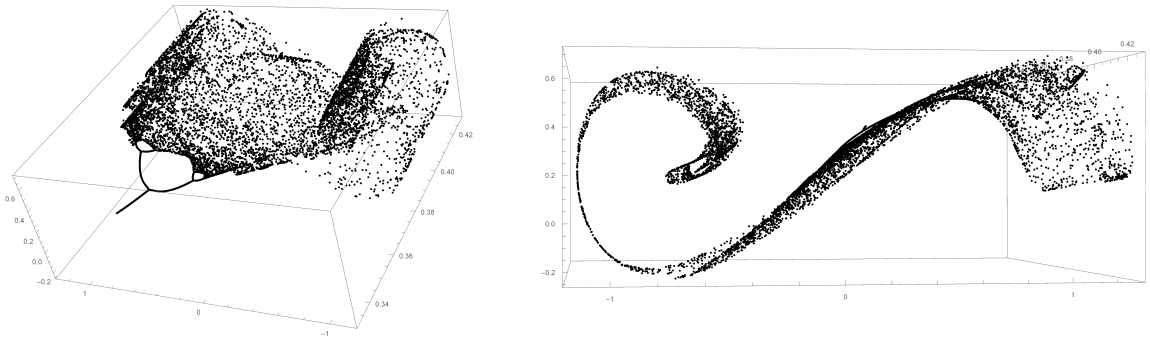

Figure 4.5: 3D phase space plot of the cascade of the Duffing Oscillator via the full Poincaré section for $a \to 0.5, b \to -1$.

4.4 Basin Boundaries

During the transition to chaos, the **basin boundaries** also undergo interesting transformations. The *basins of attraction* are the subsets of phase space for which the system approaches one of the fixed points. As has been demonstrated by the periodic orbits of the Duffing Oscillator, these limit cycles will either be around the positive or negative sink. What is interesting is how the boundaries of the basins of attraction evolve during the transition to chaos.

Figure 4.6 shows this transition. For $F = 0.035$, these basin boundaries are given by the stable manifold of the unstable saddle at the origin, the boundaries being the stable manifold in Figure

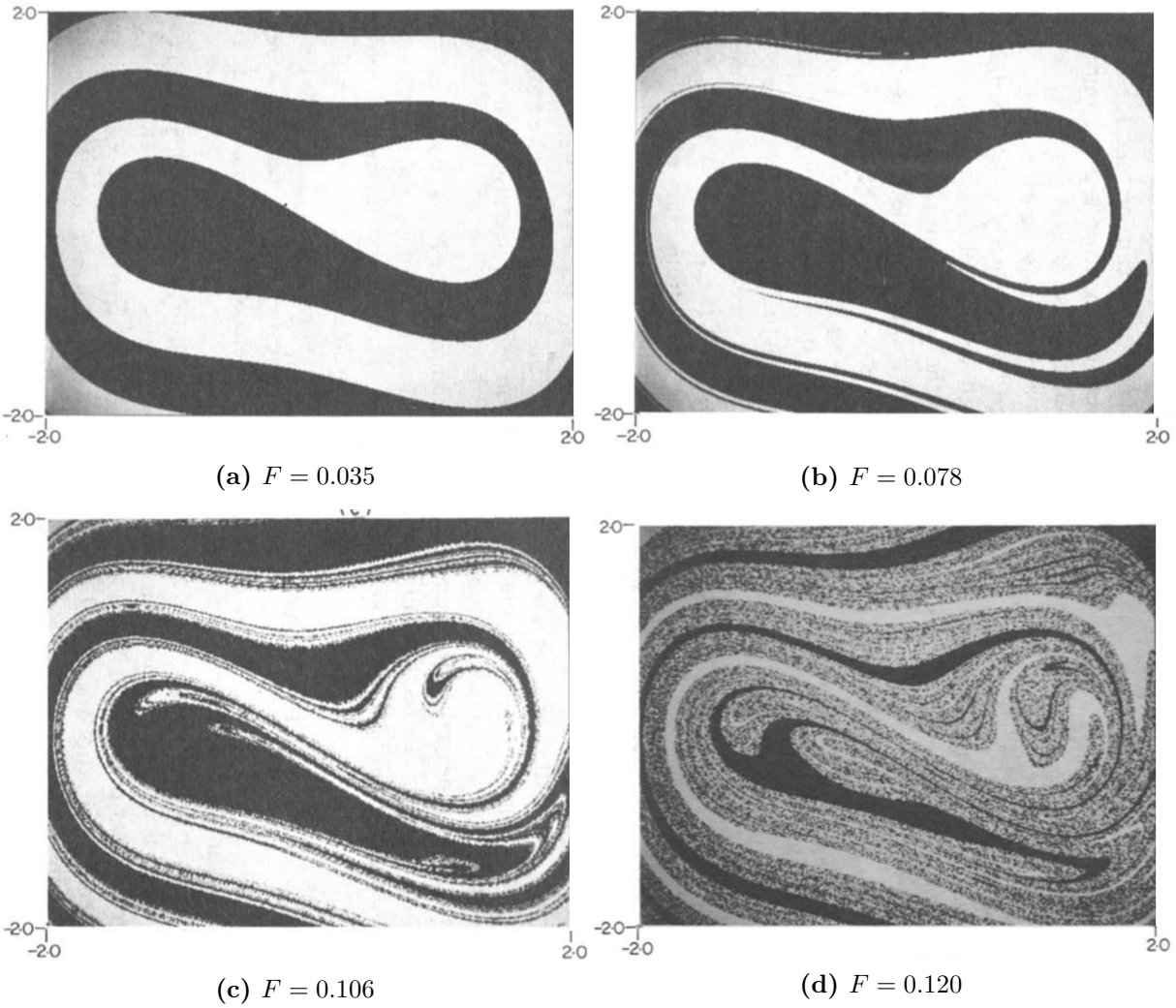

(a) $F = 0.035$ **(b)** $F = 0.078$

(c) $F = 0.106$ **(d)** $F = 0.120$

Figure 4.6: Basin boundary fractalisation during the transition to chaos with $a \to 0.168$, $b \to -0.5$ (Pezeshki & Dowell, 1987).

3.2(a). This is pre-bifurcation so the system only has its natural fixed points. However as the forcing value is increased, these boundaries begin to warp and incur on each other. At $F = 0.078$, the basin boundaries are still smooth and well defined, however each basin is beginning to incur on the other and no longer forms the symmetric spiral. The incursion increases for increasing forcing amplitude and is a sign of the cascade.

However at $F = 0.106$, the basin boundary has significantly changed. The boundary is no longer smooth but rather demonstrates a fractal structure. The heads and spiral structure of the original stable manifold can still be seen however the incursion has increased. For further increasing values of F, $F = 0.120$ for example, this structure begins to disintegrate and the basins of attraction plot approaches static noise. At this point, the transition is complete.

According to Ott (2002, p. 335), this transition from a smooth boundary to a fractal boundary occurs discontinuously and is called **basin boundary metamorphosis**. This change occurs due to the formation of homoclinic intersections described in Section 3.3. Homoclinic points generate chaotic motion and the jump from a smooth boundary to a fractal boundary occurs somewhere during the period doubling cascade. Thus it is reasonable to conclude that these three events, the fractalisation of the boundary basins, the formation of a homoclinic intersection and the limit of uncountably infinite period doubling all occur for the same F value and mark the transition to chaos.

5 Chaos

Now that the concept of attractors, orbits and the route to chaos has been explored, this section concerns itself with quantitative measures of chaotic motions. But first a definition of chaotic motions is needed. Because the majority of chaotic systems are analysed through computational numerical approximations, it is actually nigh impossible to prove if a system is in fact exhibiting chaotic behaviour or is simply a periodic orbit with really large k. For practical purposes, the difference is negligible and thus physicists don't often concern themselves with it.

Instead, chaotic systems are characterised by the concept of **sensitivity to initial conditions** in finite phase space. This describes the phenomena where slightly varying the initial conditions produces large changes in the system with time such that the system is theoretically fully determined but practical prediction is basically impossible. Note that the restriction of finite phase space is to exclude systems that just diverge from a point. Heuristically this is an intuitive definition of chaos, however to be useful it needs to be formalised. This is the aim of Lyapunov exponents.

5.1 Lyapunov Exponents

Formally, if a system is chaotic, then orbits which differ slightly in phase space initially should diverge exponentially over time such that $d(t) = d_0 \exp(\lambda t)$ where λ is the Lyapunov exponent. This definition works well for short time scales but since the phase space is finite, it cannot continue. Hence instead consider the limiting definition for the Lyapunov exponent.

$$\lambda = \lim_{t\to\infty} \lim_{d_0\to 0} \frac{1}{t} \ln\left(\frac{d(t)}{d_0}\right) = \lim_{t\to\infty} \frac{1}{t} \ln\left(D_x f^t(x) \cdot y\right) \tag{5.1}$$

Note that the limit as $d_0 \to 0$ merely is the change in the function so the Jacobian definition has also been included where x and y are the paths examined.

Supposing that this limit is well defined (that is that d_0 approaches 0 faster than t approaches infinity), then it can be used to characterise the separation along orthogonal dimensions in phase space. Thus for a three dimensional system like the Duffing Oscillator, the Lyapunov spectrum should consist of three Lyapunov exponents.

Calculating Lyapunov exponents for dynamical systems is not trivial as most do not have analytic solutions. Sandri (1996) has created a Mathematica Package that calculates the Lyapunov exponents for a variety of systems. Table 2 shows some of the Lyapunov exponents for different

Table 2: The two Lyapunov Exponents for various forcing amplitudes with $a \to 0.5,\ b \to -1$.

F	λ_1	λ_2
0.1	-0.24967	-0.25033
0.35	-0.10304	-0.39696
0.36	0.0535732	-0.553573
0.7	0.15979	-0.65979

forcing amplitudes. For F of very low values, the Lyapunov exponents are highly negative and so nearby orbits are actually attracted together which is in keeping with the idea of them decaying to a period 1 attractor. During the bifurcation (like at $F = 0.35$), the Lyapunov exponents are still negative indicating attractors but are less powerful. By $F = 0.36$, the system has transitioned to chaotic behaviour and λ_1 is positive indicating chaos whilst for $F = 0.7$, λ_1 has

increased threefold and inducing a 20 fold increase in the chaotic motion. Note that there exists a λ_3 exponent associated with the third dimension but since this is the trivial time equation $\dot{t} = 1$, it is constantly zero.

5.2 Chaotic Attractors

In Section 4, it was suggested that the attractors of the period k orbits increased to infinite with the cascade. This is what generates a **chaotic attractor** which, as it's name suggest, is the limiting cycle for chaotic motion. However an attractor is dense in phase space which

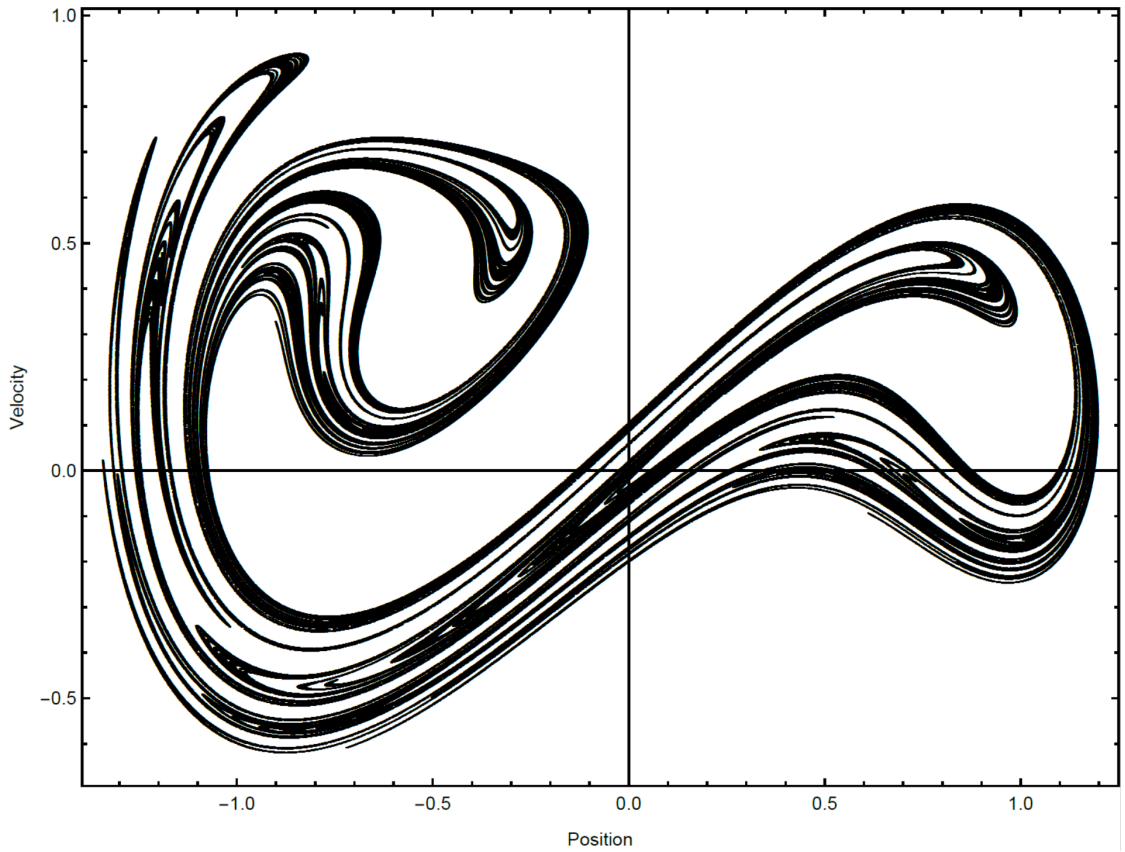

(a) $a \to 0.08,\ b \to -0.8,\ F \to 0.2$. One million points are plotted.

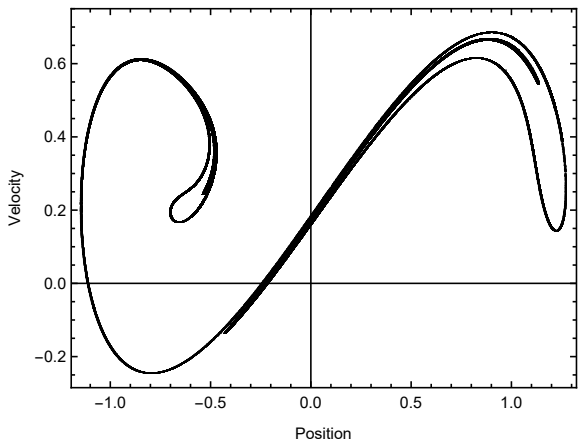

(b) $a \to 0.5,\ b \to -1,\ F \to 0.4$.

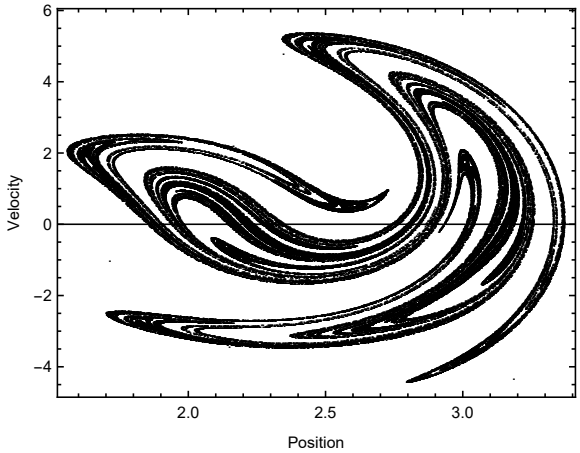

(c) $a \to 0.05,\ b \to 0,\ F \to 7.5$.

Figure 5.1: A selection of Chaotic Attractors.

means it has an uncountably infinite periodicity so never repeats. What can be said is that after substantial evolution, the system will be found on the chaotic attractor. In Figure 5.1 there are a variety of different chaotic attractors for the Duffing Oscillator. Each attractor is unique and changes based on the parameters given.

Chaotic attractors are dense because they are **fractals**. A fractal is any geometrical object which has the same structure given successive magnification; it does not simplify. Figure 5.2 demonstrates this magnification and how it preserves the complexity of the structure. Self

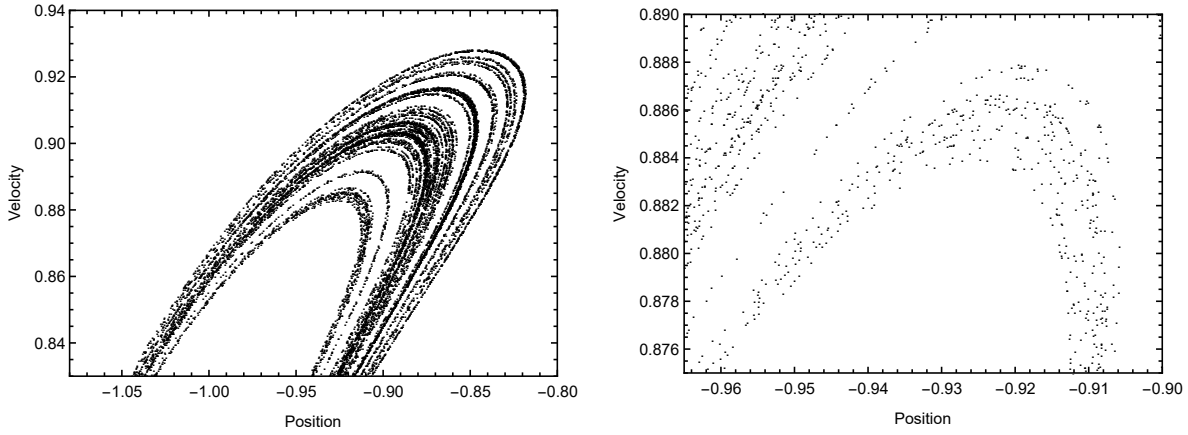

(a) The top left tongue.

(b) The bottom band of Figure 5.2(b).

Figure 5.2: Magnifications of the top left tongue of the Chaotic attractor in Figure 5.1(a)

similarity alone seems a somewhat arbitrary and heuristic definition for a fractal so instead physicists talk about the **fractal dimension** of a fractal. The problem lies in the fact that there are many different ways to calculate the fractal dimension and all give subtly different answers. Fundamentally, the fractal dimension is a dimension, if you calculate the fractal dimension for a square the answer is two and for a line it is one. Naturally, this dimension only makes sense for integers. Fractals are those geometric objects with non-integer dimensions.

One way to calculate the fractal dimension is the *box counting* method. The box counting dimension is defined by

$$\text{boxdim} = \lim_{\varepsilon \to 0} \frac{\ln(N(\varepsilon))}{\ln(1/\varepsilon)} \tag{5.2}$$

where ε is the length of a n dimensional hypersquare and $N(\varepsilon)$ is the number of such hypersquares required to cover the fractal (Alligood et al, 1996, p. 174). It says that the dimension of the fractal is the limit of the log ratio between the number of boxes and the inverse length of said boxes or more intuitively that the number of boxes is given by $N(\varepsilon) = C(1/\varepsilon)^d$. Alligood et al. (1996, p. 175-7) show that constants are negligible for small ε, that any sequence of boxes will suffice and that the 'boxes' can be any shape that can cover the fractal.

To get an estimate of this limit, a Log-Log plot can be constructed and the linear model for decreasing ε values will give a good approximation to the dimension. By choosing $\varepsilon = 2^{-n}$, this task is largely simplified as then the plot of $\log_2(N(2^{-n}))/-n$ approximates the dimension d. This is seen in Figure 5.3(a) where the linear model has the equation $y = 1.602x + 2.719$. Thus the box counting dimension of fractal 5.1(a) is boxdim $= 1.602$. This is non integer as expected and thus the chaotic attractor is clearly fractal.

Another method of calculating the fractal dimension is the *correlation dimension* which pairs points together and looks at their limiting ratio. It is attractive because it is defined primarily

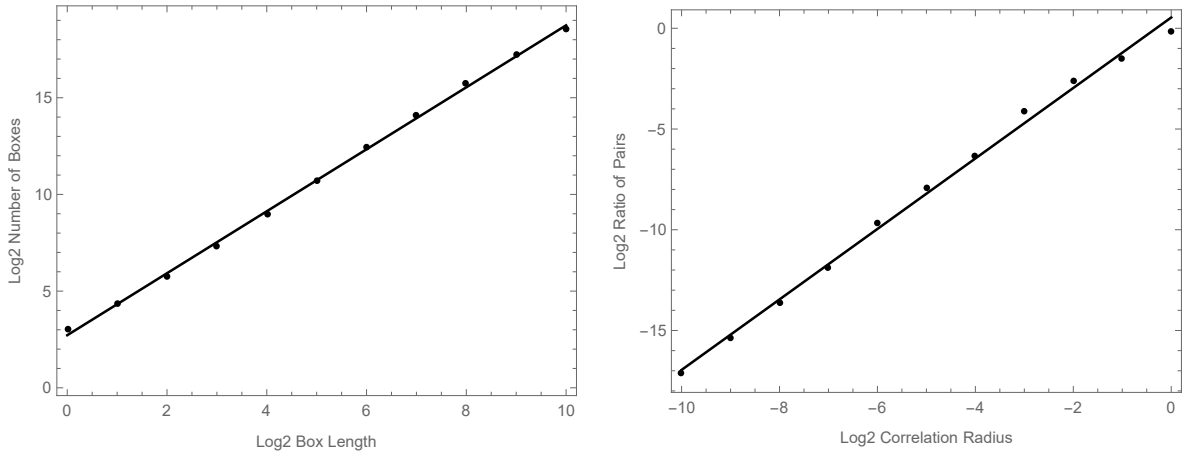

(a) Box counting. **(b)** Correlation.

Figure 5.3: An approximation to the fractal dimension for Figure 5.1(a) via two methods.

for the orbit of a dynamical system. In particular, define the correlation function

$$\mathrm{Cor}(r) = \lim_{N\to\infty} \frac{\#\{\text{pairs } w_1, w_2 : |w_1 - w_2| < r\}}{\#\{\text{pairs } w_1, w_2\}} \tag{5.3}$$

where $w_{1,2}$ are pairs in the Poincaré section and N is the iterations of the time-2π map. Then the correlation dimension is given by

$$\mathrm{cordim} = \lim_{r\to 0} \frac{\ln(\mathrm{Cor(r)})}{\ln(r)}. \tag{5.4}$$

Again $r = 2^{-n}$ is chosen to approximate the limit thus providing a linear model on $\log_2(\mathrm{Cor}(2^{-n}))/-n$. This is demonstrated in Figure 5.3(b) where the linear model has the equation $y = 1.749x + 0.5357$. Thus the correlation dimension of fractal 5.1(a) is cordim $= 1.749$. As evident this is slightly different from the box counting dimension ($|\mathrm{bd} - \mathrm{cd}| = 0.147$). Both however are non-integer and are roughly approximate and thus it can be concluded the chaotic attractors are definitely fractals.

5.3 Evolution of the Poincaré Section

So far the Poincaré section has been viewed with the surface of a section $t = 0 \mod 2\pi$ however just as valid a section could be produced for any $n \in [0, 2\pi]$ giving $t = n \mod 2\pi$. Producing such a section will show how the chaotic attractor evolves through its 2π period and show the repetition over the 2π period.

An animation was constructed which shows this evolution and is included in the attached Mathematica notebooks. Figure 5.4 shows six evenly spaced snapshots from this animation. As evident, the lobes and the tongues stretch and morph in a fractal manner. Sections of the lobe are stretched whilst others are folded but the overall structure remains the same. This is another demonstration of the self similarity of the chaotic attractor as lobes are magnified and stretched despite maintaining the same dense structure. In fact the section is topologically identical after a 2π evolution.

The lobes of the Poincaré section also appear to evolve around the stable fixed points of the Duffing potential, $(\pm\sqrt{b}, 0)$. Whilst this motion is no where near as regular as the limiting cases discussed in Section 2.2, the attractive power of these wells is clear as it keeps the chaotic orbit in a finite phase space and focus's the time evolution around the stable points of the wells.

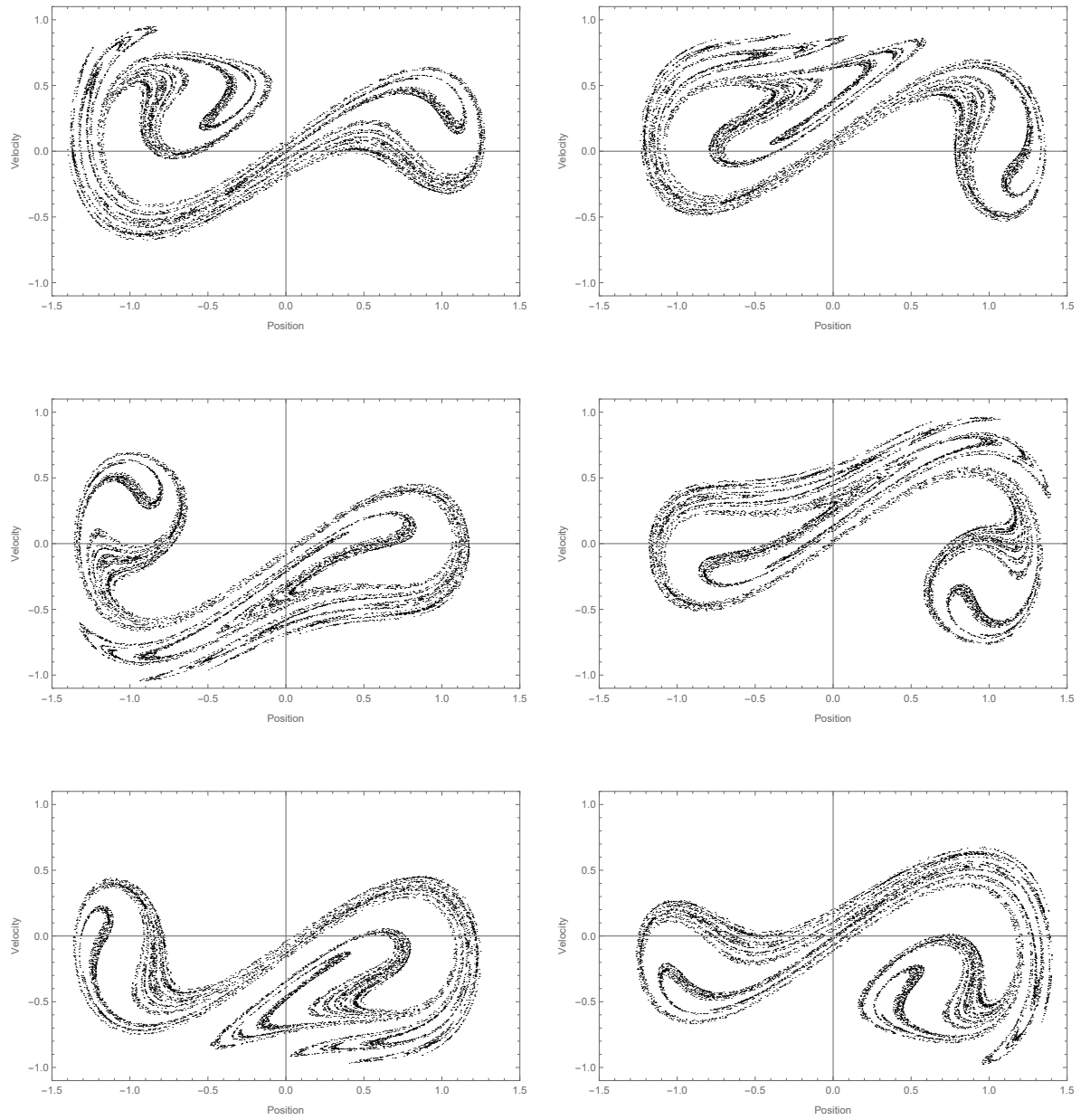

Figure 5.4: Snapshots of the time evolution of a Poincaré section animation. Angle rotates clockwise around in increments of $\pi/3$.

Not every attractor shows evidence of this potential, attractor 5.1(c) has a symmetric potential which is purely cubic. The evolution is actually much more complicated and the centre of the attractor oscillates back from $x = 2.5$ to $x = -2.5$. This more erratic behaviour is probably due to the larger forcing to damping ratio.

6 Conclusion

In this report, a nonlinear dynamic system, the Duffing Oscillator, has been extensively examined to demonstrate the principles of chaotic motion. Limiting cases have been investigated to show how the Duffing Oscillator collapses to well known standard oscillations like damped and nondamped nonlinear oscillations. The nonlinearity of the frequency response profile was examined to show the hysteric dependence of the system on the forcing frequency.

Fixed points of the system were investigated and it was shown that the Duffing Oscillator has two sinks and an unstable saddle. Analysis of stable manifolds and their intersections with unstable manifolds, called homoclinic points, revealed a sufficient condition for chaos to occur.

Periodic orbits were then defined which naturally lead to the concept of bifurcations, both saddle-node and period doubling. Since it always has a stable fixed point for low forcing, it was identified that the Duffing Oscillator only undergoes period doubling bifurcations. The concept of a cascade was presented as repetitive period doubling which lead to chaos as the period approached an uncountable infinity which was ultimately the chaotic attractor. The fractalisation of the basin boundaries was then investigated to demonstrate this transition to chaos.

Finally chaotic motions were quantified using Lyapunov exponents and the Lyapunov exponents were derived for a variety of forcing amplitudes to explain the route to chaos. Chaotic attractors were then presented using the Poincaré section. Their fractal nature was then determined by a demonstration of self similarity and the calculation of the box counting fractal dimension and the correlation dimension. Finally, the evolution of the Poincaré section showed how the folding and stretching of the attractor left it topologically identical, further cementing the dense fractal nature of the chaotic attractor.

Thus the Duffing Oscillator has provided a very rich example to demonstrate many important techniques for characterising chaotic motions.

References

[1] Alligood KT, Sauer TD & Yorke, JA. 1996. *Chaos An Introduction to Dynamical Systems.* 1st edn, Springer.

[2] Berger, J.E. & Nunes, G. 1997. 'A mechanical Duffing oscillator for the undergraduate laboratory.' *American Journal of Physics*, vol. 65, p. 841-6.

[3] Corr, C. 2015. *Second Year Laboratory Manual.* Physics Education Centre, College of Physical and Mathematical Sciences, the Australian National University, Canberra.

[4] Das S, Bhattacharyya J, & Mohapatra SRP. 2002. *The Duffing Oscillator: A system with Cubic Nonlinearity.* http://satyanarayanray.tripod.com/duffing.pdf

[5] Kanamaru, T. 2008. 'Duffing oscillator.' Scholarpedia. http://www.scholarpedia.org/article/Duffing_oscillator

[6] Kulkarni VS. 2012. 'Complexity, Chaos, and the Duffing-Oscillator Model: An Analysis of Inventory Fluctuations in Markets.' *Cornell University Library, arXiv.*

[7] Lenci, S. & Rega, G. 2011. 'Chapter 7: Forced harmonic vibration in a Duffing oscillator with negative linear stiffness and linear viscous damping.' *The Duffing Equation: Nonlinear Oscillators and their Behaviour.* John Wiley & Sons.

[8] Massachusetts Institute of Technology. 2013. *The Buckingham Pi Theorem in Dimensional Analysis.* http://ocw.mit.edu/courses/mechanical-engineering/2-25-advanced-fluid-mechanics-fall-2013/dimensional-analysis/MIT2_25F13_The_Buckingham.pdf

[9] Massachusetts Institute of Technology. n.d. *Fluids - Lecture 4 Notes.* http://web.mit.edu/16.unified/www/FALL/fluids/Lectures/f04.pdf

[10] Moon, F.C. 1992. *Chaotic and Fractal Dynamics.* 1st edn, Wiley, New York.

[11] Nardone, P. 1995. 'Re: Box counting dimension for fractals via Mathematica??' *MathGroup Archive.* http://forums.wolfram.com/mathgroup/archive/1995/Dec/msg00401.html

[12] Ott, E. 2002. *Chaos in Dynamical Systems.* 2nd edn, Cambridge University Press.

[13] Pezeshki, C. & Dowell, E.H. 1986. 'An Examination of Initial Condition Maps for the Sinusoidally Excited Buckled Beam Modelled by the Duffing's Equation.' *Journal of Sound and Vibration,* vol. 117, p. 219-232.

[14] Sandri, M. 1996. 'Numerical Calculation of Lyapunov Exponents.' *The Mathematica Journal,* vol. 6, no. 3, p. 79-84.

[15] Sconza, A. & Torzo, G. 2002. 'The torsion pendulum as a tool to study non-linear oscillations and the transition to deterministic chaos.' *Physics Department "G Galleli".* Padova Univeristy, Italy.

[16] Sethna, J. 1994. *What's Hysteresis?* Laboratory of Atomic and Solid State Physics, Cornell University. http://www.lassp.cornell.edu/sethna/hysteresis/WhatIsHysteresis.html

[17] Sprott, J.C. 2003. *Chaos and Time-Series Analysis.* 1st edn, Oxford University Press.

[18] Srebro, R. 1995. 'The Duffing oscillator: a model for the dynamics of the neuronal groups comprising the transient evoked potential.' *Electroengephalongr. Clin. Neurophysiol.* vol. 96, p. 561-573.

[19] Weisstein, EW. n.d. "Linear Stability." From MathWorld-A Wolfram Web Resource. http://mathworld.wolfram.com/LinearStability.html

[20] Zhao, F. 2014. *Chaotic behaviour of the Duffing Oscillator.* https://frankzhao.com.au/duffing_frank_zhao_web.pdf